THE JOURNAL OF BIOLOGICAL CHEMISTRY VOL. 288, NO. 50, pp. 35660–35670, December 13, 2013

Bile Acids Modulate Signaling by Functional Perturbation of Plasma Membrane Domains*

Received for publication, September 16, 2013, and in revised form, October 21, 2013 Published, JBC Papers in Press, October 28, 2013, DOI 10.1074/jbc.M113.519116

Yong Zhou[‡1], Kelsey N. Maxwell[‡], Erdinc Sezgin[§], Maryia Lu[‡], Hong Liang[‡], John F. Hancock[‡], Elizabeth J. Dial[‡], Lenard M. Lichtenberger[‡], and Ilya Levental[‡2]

From the [‡]Department of Integrative Biology and Pharmacology, the University of Texas Medical School, Houston, Texas 77030 and the [§]Max Planck Institute for Molecular Cell Biology and Genetics, Dresden, Germany 01307

Background: Bile acids (BAs) affect cellular membranes.
Results: BAs stabilize domains in plasma membranes, leading to reorganization of membrane proteins and signaling perturbations.
Conclusion: BAs affect cell function by modulating the stability of plasma membrane nanodomains.
Significance: These results suggest mechanisms for regulation of functional membrane domains and nonreceptor-mediated BA signaling.

Eukaryotic cell membranes are organized into functional lipid and protein domains, the most widely studied being membrane rafts. Although rafts have been associated with numerous plasma membrane functions, the mechanisms by which these domains themselves are regulated remain undefined. Bile acids (BAs), whose primary function is the solubilization of dietary lipids for digestion and absorption, can affect cells by interacting directly with membranes. To investigate whether these interactions affected domain organization in biological membranes, we assayed the effects of BAs on biomimetic synthetic liposomes, isolated plasma membranes, and live cells. At cytotoxic concentrations, BAs dissolved synthetic and cell-derived membranes and disrupted live cell plasma membranes, implicating plasma membrane damage as the mechanism for BA cellular toxicity. At subtoxic concentrations, BAs dramatically stabilized domain separation in Giant Plasma Membrane Vesicles without affecting protein partitioning between coexisting domains. Domain stabilization was the result of BA binding to and disordering the nonraft domain, thus promoting separation by enhancing domain immiscibility. Consistent with the physical changes observed in synthetic and isolated biological membranes, BAs reorganized intact cell membranes, as evaluated by the spatial distribution of membrane-anchored Ras isoforms. Nanoclustering of K-Ras, related to nonraft membrane domains, was enhanced in intact plasma membranes, whereas the organization of H-Ras was unaffected. BA-induced changes in Ras lateral segregation potentiated EGF-induced signaling through MAPK, confirming the ability of BAs to influence cell signal transduction by altering the physical properties of the plasma membrane. These observations suggest general, membrane-mediated mechanisms by which biological amphiphiles can produce their cellular effects.

Bile acids are synthesized from cholesterol in the liver, stored in the gallbladder, and secreted into the small intestines as a component of enterohepatic circulation. A hallmark characteristic of bile acids is their amphiphilicity, which determines their detergent properties and affinity for dietary lipids, facilitating intestinal absorption of these lipids in the form of mixed micelles (1–6). Because of this detergent effect, high concentrations of bile acids have been used extensively as membrane lysis agents in molecular cell biology. At sublytic doses, bile acids have been shown to influence cell signaling by specifically interacting both with nuclear receptors (7) and cell surface transporters (8). However, the fact that these biological amphiphiles interact strongly with lipids led us to the hypothesis that bile acids can influence signaling elements on the cell surface by partitioning directly into the plasma membrane and altering its microenvironment.

Recent advancements in the understanding of plasma membrane heterogeneity suggest that the plasma membrane microenvironment directly and dynamically regulates cell signal transduction (9–11). Membrane proteins interact with lipids and the actin cytoskeleton to form signaling domains on the plasma membrane, the composition and integrity of which can regulate membrane protein organization and function (10, 12–15). A subset of these domains, the lipid rafts, is driven by lipid immiscibility in the plane of the bilayer (16–18). The physicochemical principle behind this immiscibility is the preferential interactions between certain lipid species: cholesterol, sphingolipids, and fully saturated phospholipids, whose chemistries and geometries allow efficient packing into relatively ordered domains that exclude more bulky membrane components. These bulky lipids, such as branched and polyunsaturated lipids, form coexisting, relatively disordered domains (19). This immiscibility gives rise to coexistence of two liquid membrane phases in model bilayers (16, 18) and isolated bio-

* This study was supported, in whole or in part, by National Institutes of Health Grant 0GM066717 (to. J. F. H.). This work was also supported by Pilot and Feasibility Grant P30 DK56338 from the Texas Medical Center Digestive Diseases Center (to Y. Z.) and Cancer Prevention and Research Institute of Texas Grant R1215 (to I. L.). L. M. L. is a founder and shareholder of PLx Pharma Inc., Houston TX.
[1] To whom correspondence may be addressed: Suite R382, 6431 Fannin St., Houston TX 77030. Tel.: 713-500-7056; Fax: 713-500-7444; E-mail: yong.zhou@uth.tmc.edu.
[2] To whom correspondence may be addressed: Suite 4.202, 6431 Fannin St. Houston, TX 77030. Tel.: 713-500-5566; Fax: 713-500-7444; E-mail: ilya.levental@uth.tmc.edu.

logical membranes (20, 21), and these have been used as a model for cholesterol-dependent domains in live cells (for review, see Refs. 19, 22–26).

Phase separation into coexisting lipid-driven domains of varying compositions and physical properties can be observed in plasma membranes isolated from live cells, termed giant plasma membrane vesicles (GPMVs)[3] (21, 27). Conceptually, the observation of two coexistent, lipid-driven, liquid phases in a membrane that maintains the lipid and protein diversity of the native plasma membrane provides a critical validation of the raft hypothesis. Practically, the large size (up to 10 μm), equilibrated nature, and microscopic phase separation of these vesicles allow examination of the properties and compositions of raft domains by fluorescence microscopy, in isolation from the confounding variables of live cells (20, 21, 27–31).

The stable, long lived microdomains in isolated membranes are reflective of the nanoscale segregation of live cell membranes (10, 12, 32). Such nanoscale organization has been observed by spectroscopy (33–35) and electron microscopy (36, 37) as small (tens of nanometers), highly dynamic (lifetime $<$1 s) proteolipid nanodomains, referred to as nanoclusters (12, 38). Like lipid rafts, these nanoclusters depend on lipids, including cholesterol, for their lateral segregation (37). These clusters can be essential for the activity of proteins embedded therein, *e.g.* the small GTPase Ras proteins only bind downstream effectors and propagate signal transduction from nanoclusters (39–41).

Amphiphilic agents (*e.g.* nonsteroidal anti-inflammatory drugs) have been shown to affect proteolipid nanoclustering in cell membranes coincident with their reorganization of model membranes consisting only of synthetic lipids (33, 42, 43). Bile acids (BAs), as biological amphiphiles, can also intercalate into lipid membranes and alter lipid distribution (44, 45). Further, the signaling effects of bile acids correlate with their hydrophobicity and thus their membrane affinity (46). Therefore, BAs have the potential to affect cell signaling by perturbing the organization of the plasma membrane, although there is no direct evidence for such membrane-mediated effects of BAs on signaling components at the cell surface.

In this study, we have systematically examined the interaction between the unconjugated bile acids cholic and deoxycholic acid (CA and DCA, respectively) and biological/biomimetic membranes, from fully synthetic liposomes to live cell plasma membranes. We observed solubilization of model and natural membranes, correlating with cellular toxicity, at BA concentrations near the critical micellar concentration (cmc), which may approximate their levels in the lumen of the small intestine in certain pathophysiological conditions. At subtoxic (order of magnitude smaller than cmc) doses, BAs alter domain properties in isolated plasma membranes and synthetic liposomes, reflected in a reorganization of intact cell plasma membranes quantified by Ras nanoclustering. These effects on the organization of Ras lead to alterations in the efficiency of EGF-stimulated MAPK signaling. Thus, bile acids alter cell surface signaling activities by modulating the stability of lateral domains and thereby changing distribution of lipids and proteins in the plasma membrane.

EXPERIMENTAL PROCEDURES

Chemicals, Reagents, Cell Culture, and Plasmids—All chemicals and bile acids were purchased from Sigma. FAST DiO and FAST DiI were from Invitrogen; NBD-lithocholic acid, DOPC, DPPC, POPC, and cholesterol were from Avanti Polar Lipids. Plasmids for TfR-GFP, trLAT, and GPI-GFP were described previously (28). C-Laurdan was synthesized (47) and generously shared by Dr. Bong Rae Cho.

Rat basophilic leukemia RBL-2H3 cells were cultured in media containing 60% minimum Eagle's medium, 30% RPMI 1640 medium, and 10% FBS supplemented with penicillin/streptomycin (Invitrogen) and transfected using nucleofection with reagents and protocol from Lonza. Wild-type BHK cells as well as BHK cells stably expressing GFP-K-Ras.G12V or GFP-H-Ras.G12V were cultured in DMEM containing 10% FBS. The stable cell lines were described in previous studies (33).

Liposome Leakage Assay—The detailed calcein permeability technique was described elsewhere (48). Briefly, ~6 mg of monounsaturated DOPC dissolved in chloroform was purged with nitrogen gas to evaporate chloroform and then exposed to vacuum overnight to eliminate trace amount of chloroform. The resulting lipid film was suspended in 2 ml of Tris containing 4.5 mM calcein. Subsequent vortexing and sonication for 10 min induced the formation of liposomes encapsulating high concentrations of calcein. The suspension containing a mix of calcein-containing liposomes and free calcein molecules was passed through a Sephadex G-50 column to separate liposomes, which elute in the void volume, from free calcein in the bulk solution. The calcein-containing liposomes were exposed to bile acid solutions dissolved in Tris for 30 min at 23 °C. Fluorescence intensity of calcein was measured (excitation, 472 nm; emission, 516 nm). The maximal fluorescent intensity of calcein was obtained by adding ~0.5% Triton X-100 to completely lyse all liposomes at the end of each experiment. The percentage of calcein leakage was calculated

$$\%\ \text{Leakage} = (F_t - F_o)/(F_{max} - F_o)*100 \qquad \text{(Eq. 1)}$$

where F_t is the fluorescent intensity of a liposome solution exposed to bile acid solutions, F_o is the control fluorescent intensity of a liposome solution before being exposed to bile acid, and F_{max} is the fluorescent intensity obtained after exposure to Triton X-100.

Lactate Dehydrogenase (LDH) Assay—Cells cultured to 85–90% confluence, washed with PBS buffer three times, and incubated in serum-free medium containing various doses of DCA or CA. After 3 h of bile acid treatment, the suspending

[3] The abbreviations used are: GPMV, giant plasma membrane vesicle; BA, bile acid; BHK, baby hamster kidney; CA, cholic acid; cmc, critical micellar concentration; DCA, deoxycholic acid; DOPC, dioleoyl phosphatidylcholine; DOPE, dioleoyl phophatidylethanolamine; DPPC, dipalmitoyl phosphatidylcholine; FLIM, fluorescence lifetime imaging microscopy; GFP-tK/GFP-tH, GFP-tagged membrane-anchoring domain of K-Ras/H-Ras; GPI, glycophosphatidylinositol; LDH, lactate dyhydrogenase; NEM, *N*-ethylmaleimide; PFA, paraformaldehyde; POPC, 1-palmitoyl-2-oleoyl-*sn*-glycero-3-phosphocholine; T_{misc}, miscibility transition temperature; TfR-GFP, transferrin receptor fused to green fluorescent protein; trLAT, transmembrane domain of linker for activation of T cells fused to red fluorescent protein.

medium was collected, and the level of a cytosolic enzyme, LDH, was measured using a LDH assay kit from Sigma-Aldrich, according to the manufacturer's instruction (49).

Giant Plasma Membrane Vesicle Labeling and Preparation—GPMVs from live rat basophilic leukemia (RBL-2H3) cells were isolated and imaged as described previously (18, 50). Briefly, cells were washed in GPMV buffer (10 mM HEPES, 150 mM NaCl, 2 mM $CaCl_2$, pH 7.4) then incubated with GPMV buffer supplemented with 25 mM paraformaldehyde (PFA) and 2 mM dithiothreitol (DTT) (or 2 mM *N*-ethylmaleimide (NEM) alone) and incubated for 1 h at 37 °C. Prior to isolation, cell membranes were labeled with 5 μg/ml fluorescent disordered/nonraft phase marker FAST DiO for 10 min on ice. Vesicles were imaged at 40× on an inverted epifluorescence microscope (Nikon) under temperature-controlled conditions using a microscope stage equipped with a Peltier element (Warner Instruments).

Quantification of Raft Phase Partitioning and Miscibility Transition Temperatures—Raft partitioning coefficient and miscibility transition temperature (T_{misc}) were quantified as described previously (20, 27, 28). Briefly, $K_{p,raft}$ was defined as the background-subtracted ratio of raft phase fluorescence to nonraft fluorescence for any given fluorescent protein construct. The nonraft phase was identified by the highly disordered phase partitioning dyes FAST DiO (green) and FAST DiI (red).

For T_{misc}, phase separation was microscopically assessed for >50 vesicles/temperature and the fraction of phase-separated vesicles plotted against temperature was fit with a sigmoidal curve (see Fig. 2*B*). The point of the curve representing 50% phase separated vesicles was defined as T_{misc}.

C-Laurdan Quantification of Membrane Order—C-Laurdan spectroscopy of model membranes and microscopy of GPMVs have been described (27, 50, 51). For spectroscopy, liposomes were prepared by hydration of dried lipid films doped with 0.1 mol% C-Laurdan. The emission spectrum of these was measured from 400 to 550 nm after excitation at 385 nm. GP was defined as the integrated fluorescence intensity from the ordered channel (400–470 nm) minus that of the disordered channel (480–550 nm) normalized by the total intensity (sum of the two channels). For order imaging, GPMVs were labeled after isolation with 4 μM C-Laurdan and imaged as described above, except the fluorescent emission from C-Laurdan was split into two channels representing the ordered and disordered bands, which were then processed similarly to spectroscopic data to yield GP (for details, see Ref. 50).

Immunoelectron Microscopy (EM)/Spatial Mapping-Univariate K-function—Immuno-EM was performed as described in our previous studies (33, 37, 43). Briefly, intact cell plasma membrane sheets of BHK cells expressing GFP-tagged protein of interest were attached to copper EM grids, fixed with 4% PFA and 0.1% glutaraldehyde, and labeled with anti-GFP antibodies coupled to 4.5-nm gold particles. Images were acquired using a JEOL JEM-1400 transmission EM at 100,000× magnification. ImageJ was used to select a 1-μm^2 area on a plasma membrane sheet and to determine the *x* and *y* coordinates of gold particles within the selected area. The statistical analysis of Ripley's K-function was used to quantify the extent of nanoclustering of gold particles (Equations 2 and 3),

$$K(r) = An^{-2}\sum_{i\neq j} W_{ij}1(\|X_i - X_j\| \leq r) \quad \text{(Eq. 2)}$$

$$L(r) - r = \sqrt{\frac{K(r)}{\pi}} - r \quad \text{(Eq. 3)}$$

where $K(r)$ is the univariate K function for number n of gold particles in a selected area A; r is the radius of nanoclusters set between the values of 1 and 240 nm at 1-nm increments); $\|x\|$ is Euclidean distance; $1(x)$ is the indicator function (expected to be 1.0 if $\|x_i - x_j\|$ is ≤ the radius and 0 if not); and w_{ij}^{-1} is the fraction of the circumference of the circle with center x_i and radius $\|x_i - x_j\|$ contained within the selected area. $K(r)$ is then normalized to $L(r) - r$ on the 99% confidence interval estimated from Monte Carlo simulations. A value of 0 for $L(r) - r$ indicates complete spatial randomness whereas values above the 99% confidence interval of 1.0 indicate statistically significant clustering. Bootstrap tests were then used to evaluate for statistical differences between replicated treatment groups.

Fluorescence Lifetime Imaging Microscopy Combined with Fluorescence Resonance Energy Transfer (FLIM-FRET)—Fluorescence lifetime-based FRET measurements hold a number of advantages over intensity-based FRET measurements. Fluorescence lifetime is independent of experimental factors, such as excitation source, detection gain, optical loss, and variation in fluorophore concentrations. For these measurements, BHK cells expressing GFP-tagged protein of interest alone or in combination with RFP-tagged cognate protein were treated with various doses of DCA for 1 h and fixed with 4% PFA. Cells were then imaged using a 60× Plan-Apo/1.4 NA oil immersion lens mounted on a Nikon Eclipse wide-field microscope and GFP fluorescence lifetime was measured using a FLIM unit (Lambert Instrument, Roden, The Netherlands). GFP was excited using a sinusoidally modulated 3-W 497-nm light-emitting diode (LED) at 40 MHz under epifluorescence. Three individual experiments were conducted, and a total of > 60 cells were imaged, and GFP fluorescence lifetime values of whole cells were averaged, shown as mean ± S.E., and statistics were evaluated using one-way analysis of variance.

Western Blotting—BHK cells were grown to ~80% confluence, serum-starved for 2 h, incubated in serum-free DMEM containing various doses of DCA (0, 30, 50, 100, 200, and 300 μM) for 1 h, then stimulated with 2.5 ng/ml EGF for 5 min before being harvested. Whole cell lysates of 20 μg were separated by SDS-PAGE and blotted against pMEK, pERK, and pAkt. Intensity of the bands was imaged by a FluorChem Q Multiimager and quantified by densitometry. Band intensities were normalized to the average intensity of all measured conditions. Three independent experiments were conducted and are presented as means ± S.E.

RESULTS

Cell Injury and Membrane Disruption by Bile Acids—At concentrations above their cmc (DCA = 2–5 mM; CA ~ 11 mM (52)), unconjugated bile acids are widely used as biological

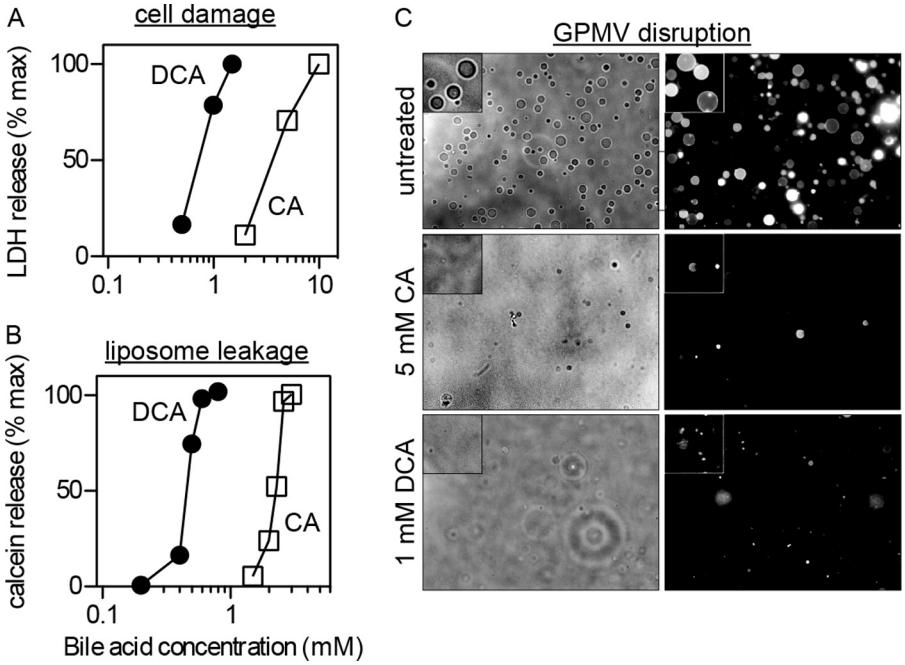

FIGURE 1. **Bile acid-induced cell injury correlates with plasma membrane vesicle dissolution.** *A*, cell toxicity quantified by leakage of the cytoplasmic enzyme LDH is sensitive to millimolar cholic and deoxycholic acid treatment. *B*, synthetic liposome leakage, measured by release of calcein, correlates with cytotoxicity. *C*, phase contrast imaging (at room temperature) of isolated GPMVs shows that treatment of GPMVs with 1 mM DCA or 5 mM CA leads to near-complete dissolution of membranes. Higher BA concentrations lead to no observable vesicles (*insets* show magnifications of representative areas). The quantitative agreement between these results strongly suggests a mechanistic link between membrane disruption and cytotoxicity. All results are representative of at least three independent experiments.

detergents for solubilization of cellular membranes. However, a variety of cellular effects have been observed with bile acid treatments well below the cmc (7, 44–46), and the mechanisms of these have not been definitively attributed. Both CA and DCA were cell injurious near their cmc, as evidenced by leakage of the cytoplasmic enzyme LDH. DCA was more toxic than CA, with maximal cell injury observed at ~1 mM compared with ~ 10 mM CA (Fig. 1*A*). To test the hypothesis that plasma membrane disruption was the mechanism behind cell injury, we evaluated the solubilizing effect of these bile acids on synthetic and natural membranes. Synthetic liposomes composed of the unsaturated phospholipid DOPC were loaded with calcein, a self-quenching fluorophore that does not fluoresce at the high concentrations encapsulated in liposomes. Membrane damage leads to release of calcein molecules into the suspending buffer, relieving self-quenching and leading to an increase in fluorescence intensity. Bile acid treatment increased calcein fluorescence intensity in a concentration-dependent manner (Fig. 1*B*), with effective concentrations similar to those inducing cell injury (Fig. 1*A*).

To confirm membrane disruption in a more realistic model of biological membranes, intact plasma membranes were isolated as GPMVs from live cells and imaged after treatment with bile acids. Transmission (Fig. 1*C*, *left*) and fluorescence (Fig. 1*C*, *right*) images of untreated GPMVs show the expected spherical morphology and approximate size distribution of this preparation (Fig. 1*C*, *top*). Bile acid treatment dramatically reduced the number of visible GPMVs, with a near-maximum response at 1 mM DCA and 5 mM CA. The size of the vesicles remaining after these treatments was also reduced.

Bile Acids Stabilize Phase Separation in GPMVs—Intriguingly, at subtoxic concentrations of bile acids (<0.6 mM for DCA), we observed a striking stabilization of phase separation in GPMVs (Fig. 2). Phase separation into coexisting, fluid, raft/nonraft domains in GPMVs was visualized by doping cell membranes with FAST DiO, a lipid fluorophore with high preference for nonraft domains (50, 53), prior to GPMV isolation. Exemplary images of vesicles demonstrating temperature-dependent phase separation are shown in Fig. 2*A*. At the lowest temperature shown (10 °C; Fig. 2*A*, *left column*) raft domains (those excluding the nonraft phase marker FAST DiO (50)) are clearly observable in all vesicles. Domains are round, diffusive, and have fluctuating edges, consistent with liquid-liquid phase separation. At higher temperatures (*right column*), untreated vesicles are uniformly fluorescent with no evidence of microscopic domains.

The temperature dependence of phase separation is quantified by microscopically assessing the percentage of phase-separated vesicles as a function of temperature, as shown in Fig. 2*B*. Sigmoidal curve fits to these data yield T_{misc}, defined as the temperature at which 50% of GPMVs are phase-separated (*dotted horizontal line*). Both BA treatments had a strong stabilizing effect on phase separation, increasing T_{misc} by up to 15 °C (Fig. 2*C*), with the effect being observed regardless of the chemical agent used to isolate GPMVs (Fig. 2*D*). Again, as for cell toxicity and vesicle disruption (Fig. 1), DCA was more effective than CA by approximately an order of magnitude.

The domain-stabilizing effects induced by treating isolated GPMVs were qualitatively reproduced by treating live cells with BAs prior to GPMVs isolation (Fig. 2*E*). The lower magnitude of the effect in live cell treatment is unsurprising, considering any number of potential cellular compensatory mechanisms (*e.g.* membrane traffic, lipid synthesis, bile acid efflux).

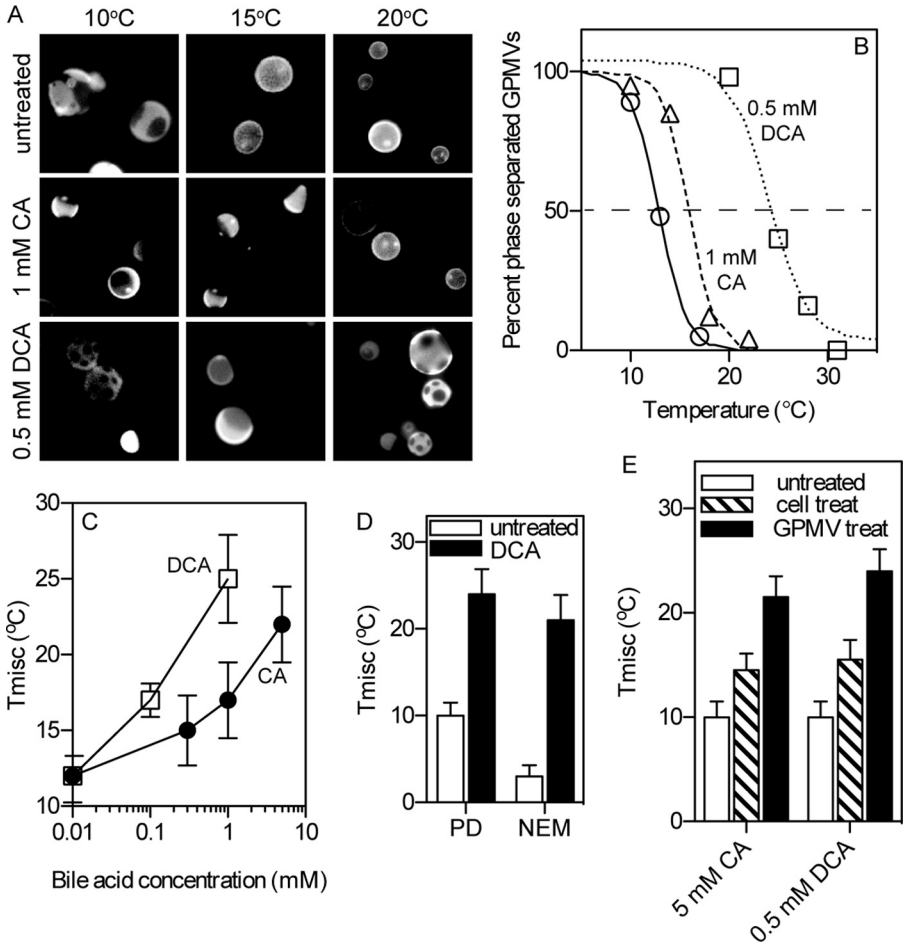

FIGURE 2. **Bile acids stabilize phase separation in GPMVs.** *A*, exemplary fluorescent images of GPMVs (labeled with FAST DiO) at various temperatures show that whereas phase separation in untreated vesicles is observable only below 15 °C, treatment with 1 mM CA increases phase separation temperature to ~17 °C and 0.5 mM DCA above 20 °C. *B*, T_{misc} is calculated by counting the percentage of phase-separated vesicles at several temperatures and fitting to a sigmoidal curve. *C*, bile acid treatment dramatically increased T_{misc}, with DCA more effective than CA. Effect of higher BA concentrations could not be evaluated because of GPMV dissolution. *D*, bile acid-mediated stabilization of phase separation was observed regardless of whether GPMVs were isolated using PFA/DTT (*PD*) or NEM. *E*, the domain-stabilizing effect of bile acids was observable (although somewhat attenuated compared with treatment of isolated membranes) by pretreating cells with BAs prior to GPMV isolation. Data in *B*--*D* are average ± S.D. (*error bars*) from three independent experiments.

Effect of Stabilization of Raft Domain Separation on Protein Partitioning—To determine whether domain stabilization would affect protein affinity for the raft phase in GPMVs, we measured the bile acid dependence of partitioning of three different fluorescent protein constructs, representing a lipid-anchored raft protein (GPI-GFP), a nonraft transmembrane protein (TfR-GFP), and a transmembrane construct with approximately equal affinity for both lipid phases (trLAT) (28). Partitioning was quantified as described previously (28), as a ratio of background-subtracted fluorescence intensity for the protein of interest in the raft *versus* the nonraft phase, defined as the raft partition coefficient ($K_{p,raft}$). The exemplary images in Fig. 3*A* demonstrate partitioning of trLAT before and after treatment of isolated GPMVs with DCA. Although a minor reduction in relative raft phase fluorescence is observable in both images and quantification in Fig. 3*B*, the effect was small and not statistically significant (regardless of GPMV isolation agent). The lack of significant differences in protein partitioning caused by DCA was consistent across all three protein constructs (Fig. 3*B*), suggesting that the stabilization of phase separation by bile acids did not dramatically affect protein partitioning between the coexisting domains.

Bile Acid Stabilizes Raft Domain Separation by Disordering the Disordered Phase—To investigate the mechanism behind the domain-stabilizing effect of DCA in GPMVs, we measured the effect of this bile acid on membrane order in natural and synthetic membranes. The order of synthetic liposomes, comprising a 1:1 molar mixture of cholesterol and DOPC, was quantified by measuring the fluorescence emission spectrum of the order-sensitive fluorophore C-Laurdan (43, 47) (Fig. 4, *A* and *B*). The ratio of red-shifted signal (centered at approximately 490 nm) and blue-shifted signal (~430 nm) yields a normalized index of membrane order known as generalized polarization (GP). DCA treatment had a highly disordering effect on the one-phase liposomes, as evidenced by the progressive red shift in the C-Laurdan emission curves (Fig. 4*A*) and reduction in generalized polarization (Fig. 4*B*). Strikingly, the disordering effect was not observed when liposomes designed to resemble the raft-mimetic liquid-ordered phase (1:1 DPPC:cholesterol) were treated with the same conditions (10 mM DCA treatments

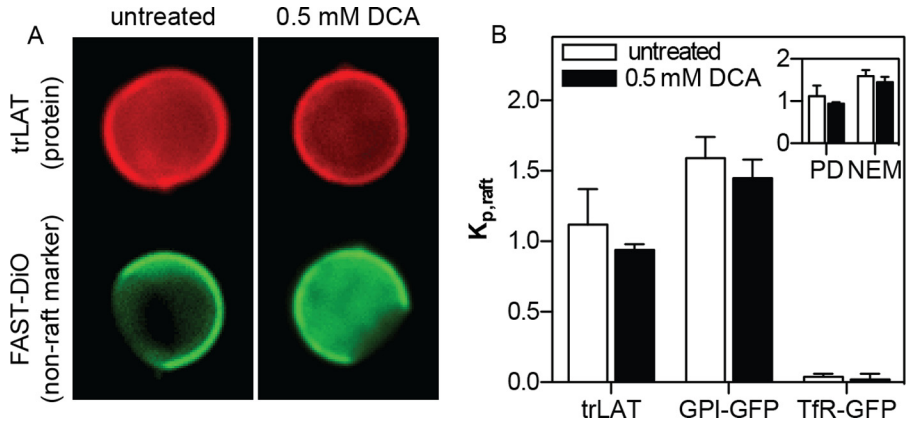

FIGURE 3. **Stabilized phase separation does not affect protein partitioning.** *A*, exemplary images of phase partitioning of a model transmembrane protein (trLAT) in untreated and 0.5 mM DCA-treated GPMVs. *Red* images show the localization of trLAT, which is approximately equal in both phases, relative to the fluorescent nonraft marker FAST DiO (*green*). *B*, partitioning quantified by $K_{p,raft}$ (the ratio of fluorescent intensity in the raft divided by nonraft phase) was slightly, but not significantly, reduced by DCA for trLAT, a peripheral raft phase protein (GPI-anchored GFP), and an integral nonraft protein (TfR-GFP). *Inset*, $K_{p,raft}$ of trLAT was not significantly different in control *versus* DCA-treated GPMVs isolated with either PFA/DTT or NEM. The higher raft phase partitioning in NEM GPMVs was expected (28). Data are mean ± S.D. (*error bars*) from 10–20 vesicles/condition, representative of three independent experiments.

are shown in Fig. 4, *C* and *D*). Large unilamellar vesicles (LUVs) with intermediate order (POPC:cholesterol at 1:1) had an intermediate response between the disordered and ordered vesicles (Fig. 4, *C* and *D*). Thus, DCA preferentially interacts with disordered membranes and makes them more disordered.

This conclusion was confirmed in biological membranes by assaying phase-separated GPMVs. The preference of bile acid for disordered *versus* ordered domains was fluorescently evaluated by incubating GPMVs prelabeled with the disordered-phase marker rhodamine-DOPE (Fig. 4*E*, *red*) with a fluorescent analog of bile acid (NBD-lithocholic acid; Fig. 4*E*, *green*). The bile acid clearly bound to the domain enriched in rhodamine-DOPE, thus confirming preferences for the more disordered/nonraft (Fig. 4*E*). We measured the result of this binding by microscopically quantifying the order of the coexisting membrane domains using Laurdan microscopy. Generalized polarization, a relative measure of membrane order, is shown color-coded in Fig. 4*F* (*cooler colors* indicative of lower GP and thus more disorder) and quantified in Fig. 4*G*. Coexisting domains of high and low order were observed (Fig. 4*F*), as expected (27, 51). DCA treatment reduced the order of the relatively disordered (*i.e.* nonraft) phase while having only a small effect (Fig. 4*G*) on the ordered, raft domain.

Bile Acid Changes Ras Nanoclustering on the Plasma Membrane and Affects MAPK Signal Transduction—To investigate the impact of domain stabilization in isolated plasma membranes (Fig. 2) on lateral membrane organization in live cells, we examined the effect of DCA on the integrity and functionality of nanodomains in intact cell plasma membranes using electron microscopy, FLIM-FRET, and Western blotting (Figs. 5 and 6).

Plasma membrane sheets were prepared and imaged by electron microscopy as described previously (36, 37). Briefly, cells were transfected with GFP-tK/GFP-tH, the GFP-tagged membrane-anchoring domain of K-Ras/H-Ras that have been established as probes for nonraft/raft nanodomains, respectively (36, 37). Plasma membrane sheets were then removed from cells by adsorption to an EM grid and labeled with an anti-GFP antibody coupled to 4.5-nm gold particles, whose distribution was quantified by Ripley's *K*-function. This function quantifies the average spatial distribution of gold particles compared with the expected density for a random distribution and reports relative clustering, $L(r) - r$, as a function of the cluster radius r, with $L(r) - r$ greater than unity as evidence of statistically significant, nonrandom clustering. Treatment with DCA markedly and dose-dependently increased GFP-tK clustering (Fig. 5*A*), in full agreement with the stabilization of nonraft domains in GPMVs (Fig. 4). Bile acid had little effect on the raft domains in GPMVs (Fig. 4, *E–G*), which was corroborated by the lack of significant effect of DCA on the clustering of GFP-tH (Fig. 5*B*).

We confirmed these electron microscopic observations of nanodomains in intact cells using FLIM-FRET (Fig. 5, *C–E*). In these experiments, reduction in the fluorescence lifetime of GFP in the presence of a FRET acceptor (here, RFP) provides evidence of intermolecular FRET and therefore protein proximity/clustering (*cooler colors* in Fig. 5*C* and *arrow* in Fig. 5*D*). The fluorescence lifetime of GFP was ~2.3 ns in BHK cells expressing GFP-tK alone and was decreased to ~2 ns in cells expressing both GFP-tK and RFP-tK as a result of energy transfer from GFP to RFP (Fig. 5, *C* and *D*). DCA led a concentration-dependent decrease in the lifetime of GFP-tK, indicative of more efficient energy transfer due to enhanced tK clustering (Fig. 5*D*). DCA had the same effect on the organization of full-length, constitutively GTP-bound, oncogenic K-Ras.G12V (Fig. 5*D*). These observations confirm that DCA-mediated reorganization of the plasma membrane affects the distribution of the nonraft marker, tK, as well as the oncogene K-Ras. Finally, consistent with liposome, GPMV, and EM data, DCA did not have a discernable effect on FRET in cells expressing GFP-tH/RFP-tH nor those expressing full-length versions of H-Ras.G12V (Fig. 5*E*).

To test the functional consequences of bile acid-induced reorganization of the plasma membrane, we examined effects of DCA on the Ras-mediated activation of the MAPK signaling cascade initiated by EGF stimulation (Fig. 6). DCA potentiated the activation (phosphorylation) of MEK, ERK, and Akt stimulated by nonsaturating doses (2.5 ng/ml) of EGF (Fig. 6). Interestingly, DCA potentiation of pMEK and pERK was much more

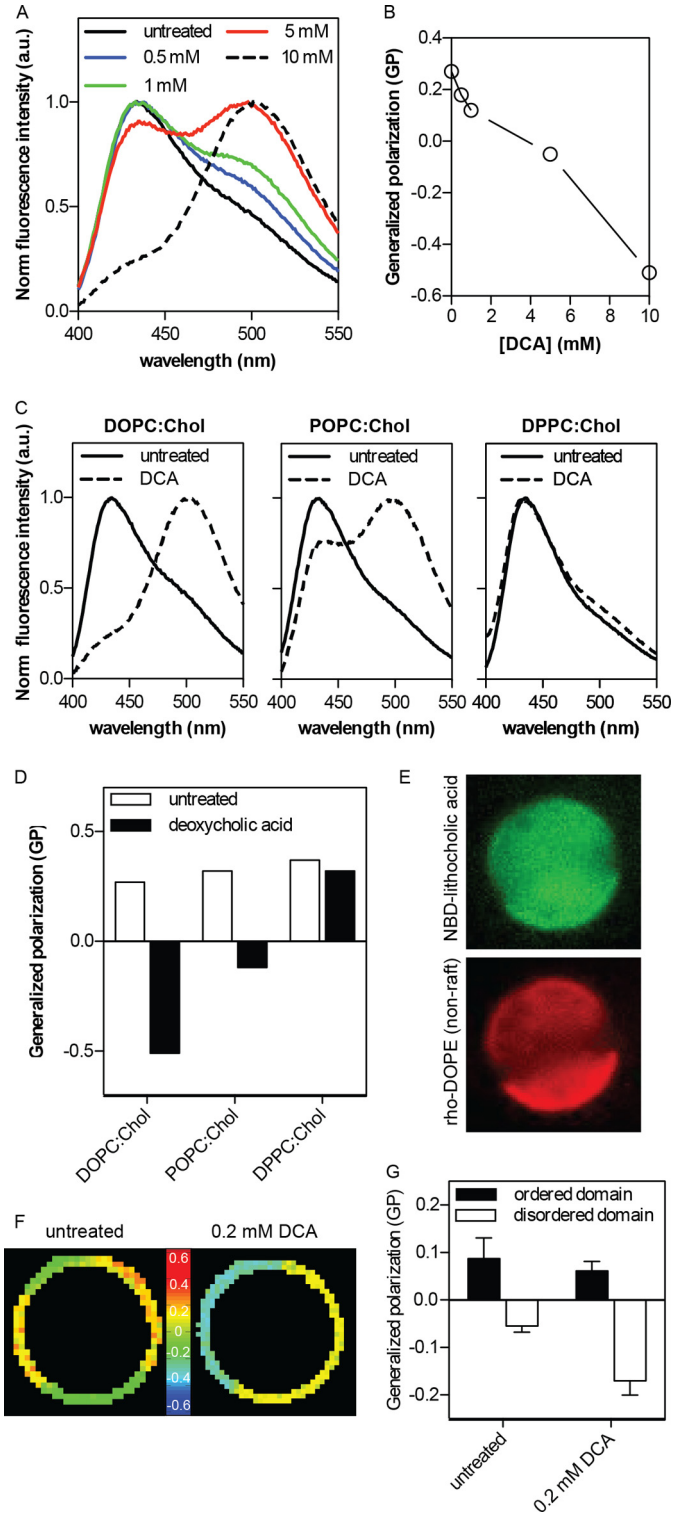

FIGURE 4. **Stabilization of domain separation by bile acid-induced disordering of the nonraft phase.** *A*, DCA induces a progressive, concentration-dependent decrease in membrane order of DOPC:cholesterol (Chol) (1:1) synthetic liposomes, as evidenced by the red shift of normalized fluorescence emission of the order-sensitive fluorophore C-Laurdan. Higher DCA concentrations are possible without complete membrane dissolution in this context because of high lipid concentration (~1 mM) relative to GPMV suspensions. *B*, generalized polarization (*GP*) of C-Laurdan calculated from the data in *A* shows the quantitative trend of membrane disordering. *C* and *D*, disordering effect of DCA is much more pronounced in liquid-disordered phase membranes (DOPC:Chol, 1:1) than liquid-ordered phase (DPPC:Chol, 1:1), with an intermediate effect on an intermediate order membrane (POPC:Chol, 1:1); *a.u.*, arbitrary units. *E*, a fluorescent analog of bile acid (NBD-lithocholic acid) preferentially binds to the disordered (nonraft) domain in phase separated GPMVs, evidenced by co-partitioning between the nonraft marker rhodamine-DOPE and the bile acid derivative. *F* and *G*, treatment of isolated GPMVs with 0.2 mM DCA leads to further disordering of the disordered domains, without a notable effect on raft phase order (mean ± S.D. (*error bars*) of 5–9 vesicles/condition). The greater difference between the coexisting domains ($\Delta GP = 0.23 \pm 0.02$ in DCA-treated compared with 0.14 ± 0.04 in untreated) is likely responsible to the DCA-enhanced stability of phase separation.

pronounced than pAkt. As K-Ras mainly regulates MEK and ERK phosphorylation whereas H-Ras more preferentially controls Akt phosphorylation (54, 55), our signaling data are fully consistent with stabilization of nonraft, K-Ras-enriched lateral membrane domains and confirm that bile acid-mediated perturbation of lateral membrane structure can lead to reorganization of membrane proteins and thereby affect the efficiency of signal transduction.

DISCUSSION

Our study systematically examined the ability of bile acids to influence lateral heterogeneity in synthetic phospholipid bilayers, isolated cell plasma membranes, and intact cells. Consistent with their well established detergent effects, cholic and deoxycholic acids near their cmc were cytotoxic (Fig. 1*A*) and efficiently disrupted synthetic membranes (Fig. 1*B*), suggesting a mechanistic connection. However, these synthetic liposomes are limited models for live cell membranes, most importantly because they lack cholesterol and integral membrane proteins, which make up a major fraction of surface area in biological membranes and contribute dramatically to their stabilities (56). However, the quantitative agreement between the onset concentration of both maximal cell injury (Fig. 1*A*) and disruption of isolated plasma membranes (Fig. 1*C*) for both bile acid treatments strongly implicates plasma membrane disruption as the mechanism of cell toxicity induced by near-cmc concentrations of BAs.

Lower doses of BAs stabilized domain formation in plasma membranes, isolated as GPMVs. Phase separation in GPMVs can be visualized by the inclusion of fluorescent dyes and/or proteins in the plasma membrane of live cells prior to vesicle isolation (21, 29, 50), providing strong evidence that intact, biological membranes have the capacity for the lipid-driven domain formation that is the central tenet of the lipid raft hypothesis (57, 58). The temperature at which separation into raft and nonraft phases can be observed varies between cell types (30) and has been shown to be sensitive to receptor-ligand binding (30) and manipulation of membrane lipid (20) and protein (27) composition. Surprisingly, the magnitude of the stabilizing effect of BAs was much larger than that induced by lipid cross-linking by cholera toxin B (4–5 °C (30)) or cholesterol depletion/loading (up to 7 °C (20)).

GPMVs have proven a particularly useful system for studying protein partitioning between coexisting raft and nonraft phases (28–30). Stabilization of phase separation in GPMVs did not have a strong effect on domain preference of three different proteins, chosen to represent the full range of raft affinity, from highly raft preferring (GPI-GFP) to completely raft-excluded (TfR-GFP) (Fig. 3). Besides being a somewhat surprising result, this observation may prove useful for observing and measuring

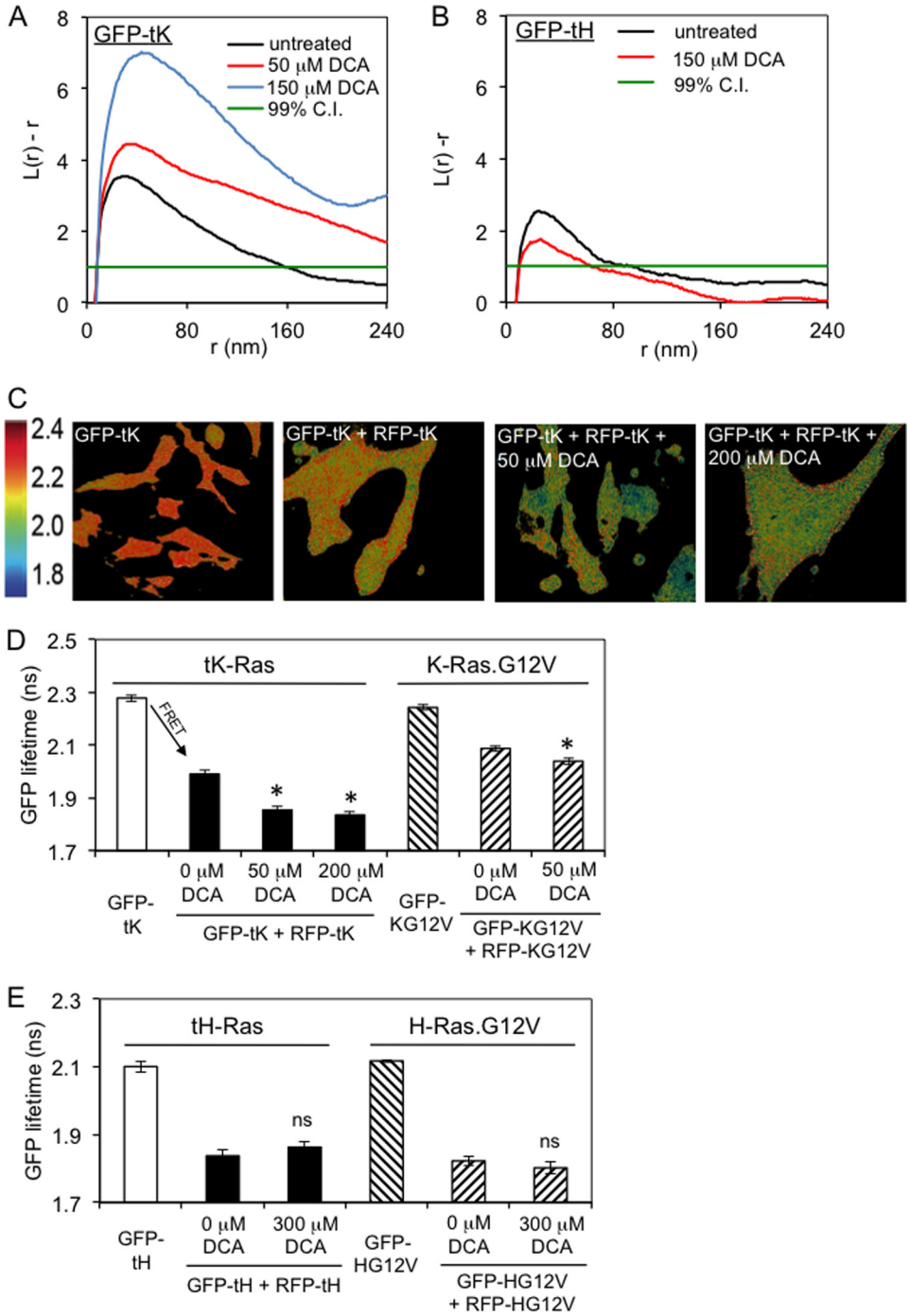

FIGURE 5. **Bile acid specifically enhances the formation of nanoclusters of GFP-tK and full-length K-Ras.** *A*, plasma membrane sheets from cells expressing GFP-tK, the GFP-tagged membrane-anchoring domain of K-Ras, were attached to EM grids and labeled with anti-GFP. Nanoclustering evaluated by EM (see "Experimental Procedures" for details of data analysis) was significantly increased in cells exposed to DCA compared with untreated controls ($p = 0.001$ for both 50 μM and 150 μM DCA). *B*, DCA at 150 μM did not have a statistically significant effect on nanoclustering of GFP-tH. *C*, representative FLIM data show fixed BHK cells expressing GFP-tK alone, or in combination with RFP-tK either untreated, treated with 50 μM, or 200 μM DCA. Images reveal a reduction of GFP lifetime with RFP coexpression due to FRET in nanoclusters and an enhancement of FRET (nanoclustering) by DCA. *D*, quantification of FLIM imaging reveals that DCA doses $\geq$50 μM significantly increased FRET (*, $p < 0.05$ compared with 0 μM DCA) indicative of enhanced nanoclustering of both the minimal anchor tK and the oncogenic full-length protein K-Ras.G12V. *E*, the clustering of tH and full-length H-Ras.G12V was not significantly affected by DCA treatment (*ns*; $p > 0.1$ compared with 0 μM DCA). All data are shown as mean $\pm$ S.E. (*error bars*) of at least $\geq$60 cells representative of three independent experiments.

partitioning of proteins without the requirement of lowering the temperature to image phase separation. It is important to note that this was not an exhaustive study of protein partitioning, and other proteins may be affected by membrane perturbations.

We identified the mechanism behind BA-mediated domain stabilization by assaying changes in the order of coexisting membrane domains. Fully consistent with recent fluorescence microscopy and spectroscopy observations (59), BAs were enriched in nonraft domains and decreased their relative order

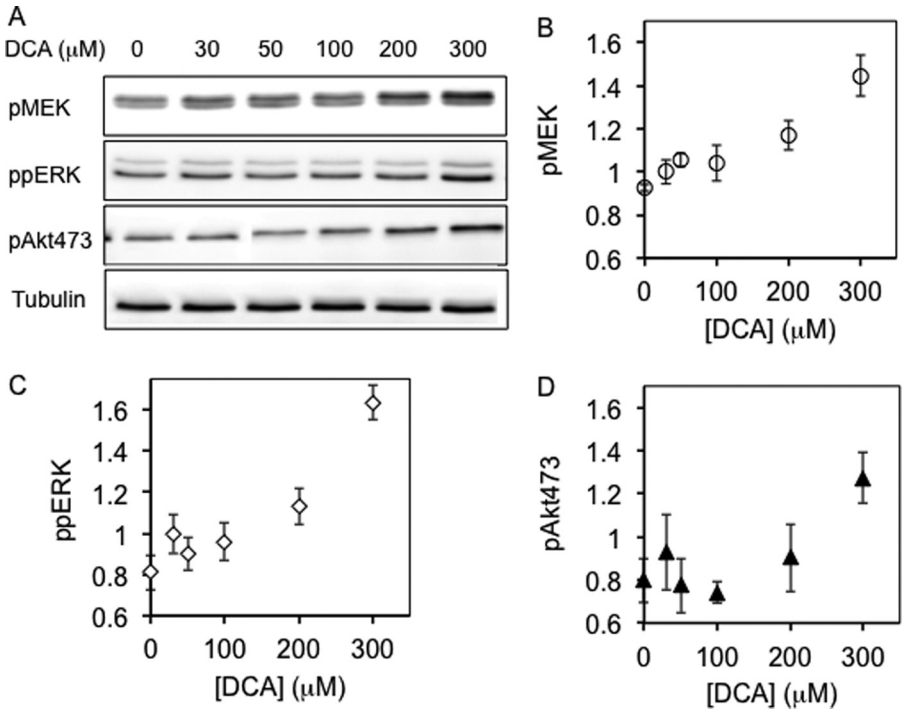

FIGURE 6. **Bile acid enhances MAPK signaling induced by EGF.** BHK cells were serum-starved for 2 h, treated with DCA for 1 h, stimulated with 2.5 ng/ml EGF for 5 min, and harvested. Whole cell lysates were used to blot for phosphorylated MEK, ERK, or Akt. *A*, representative Western blots with antibodies against pMEK, pERK, or pAkt473. *B–D*, normalized band intensity values (see "Experimental Procedures") for pMEK (*B*), ppERK (*C*), and pAkt (*D*) in the form of means ± S.E. (*error bars*) as a function of bile acid concentrations from three independent experiments.

(Fig. 4). We interpret these findings to suggest that BAs preferentially intercalate into the disordered/nonraft domains of membranes containing coexisting liquid phases, and that by doing so, they further disorder those domains relative to the more ordered ones. This disorder might be caused by BAs physically intercalating into and disrupting the packing of the disordered phase (59) or by selectively extracting lipids from the disordered phase (60). In either case, the result is a less packed disordered phase (Fig. 4*E*), enhanced immiscibility between the phases and stabilized phase separation (27). The physical mechanism behind the preferential interaction of BAs with the disordered domains is unclear, but is unlikely to be dependent on lipid headgroups, as the synthetic membrane experiments in Fig. 4 all had mixtures of PC and cholesterol.

This stabilization of domain separation in biological membranes was transduced to cellular signals by enhanced lateral segregation of the small GTPase K-Ras (Fig. 5). Nanoclustering of the nonraft partitioning lipid anchored protein K-Ras was specifically enhanced by BA treatments. Because Ras nanoclusters are the sole sites of effector binding and signal propagation (33, 37, 38, 61), the hypothesis was that DCA stabilization of nonraft nanodomains and resulting enhancement of K-Ras nanoclustering would enhance the K-Ras-regulated mitogenic signaling cascade. Indeed, BAs potentiated the K-Ras-dependent MAPK signaling cascade downstream of EGF stimulation (Fig. 6).

These results verify the relationship between phase separation in isolated GPMVs, lateral organization in intact cell membranes, and the functional consequence thereof. Additionally, our results suggest a mechanism of bile acid signaling that is alternative, and potentially complementary, to the well characterized nuclear receptor pathways (62): bile acids intercalate into cell plasma membranes and alter plasma membrane proteolipid domains, leading to modulation of protein-protein interactions and consequent signal propagation. More generally, these observations suggest that lateral membrane organization is a key regulator of cell signaling, and can be modulated by biological amphiphiles.

REFERENCES

1. Hofmann, A. F., and Hagey, L. R. (2008) Bile acids: chemistry, pathochemistry, biology, pathobiology, and therapeutics. *Cell Mol. Life Sci.* **65,** 2461–2483
2. Cabral, D. J., Small, D. M., Lilly, H. S., and Hamilton, J. A. (1987) Transbilayer movement of bile acids in model membranes. *Biochemistry* **26,** 1801–1804
3. Fullington, D. A., Shoemaker, D. G., and Nichols, J. W. (1990) Characterization of phospholipid transfer between mixed phospholipid-bile salt micelles. *Biochemistry* **29,** 879–886
4. Hofmann, A. F., and Small, D. M. (1967) Detergent properties of bile salts: correlation with physiological function. *Ann. Rev. Med.* **18,** 333–376
5. Mazer, N. A., Benedek, G. B., and Carey, M. C. (1980) Quasielastic light-scattering studies of aqueous biliary lipid systems: mixed micelle formation in bile salt-lecithin solutions. *Biochemistry* **19,** 601–615
6. Shoemaker, D. G., and Nichols, J. W. (1990) Hydrophobic interaction of lysophospholipids and bile salts at submicellar concentrations. *Biochemistry* **29,** 5837–5842
7. Zollner, G., and Trauner, M. (2009) Nuclear receptors as therapeutic targets in cholestatic liver diseases. *Br. J. Pharmacol.* **156,** 7–27
8. Dawson, P. A. (2011) Role of the intestinal bile acid transporters in bile acid and drug disposition. *Handb. Exp. Pharmacol.* **201,** 169–203
9. Young, R. M., Zheng, X., Holowka, D., and Baird, B. (2005) Reconstitution of regulated phosphorylation of FcεRI by a lipid raft-excluded protein-tyrosine phosphatase. *J. Biol. Chem.* **280,** 1230–1235
10. Lingwood, D., and Simons, K. (2010) Lipid rafts as a membrane-organizing principle. *Science* **327,** 46–50

11. Simons, K., and Gerl, M. J. (2010) Revitalizing membrane rafts: new tools and insights. *Nat. Rev. Mol. Cell Biol.* **11,** 688–699
12. Hancock, J. F. (2006) Lipid rafts: contentious only from simplistic standpoints. *Nat. Rev. Mol. Cell Biol.* **7,** 456–462
13. Sharma, P., Varma, R., Sarasij, R. C., Ira, Gousset, K., Krishnamoorthy, G., Rao, M., and Mayor, S. (2004) Nanoscale organization of multiple GPI-anchored proteins in living cell membranes. *Cell* **116,** 577–589
14. Honigmann, A., van den Bogaart, G., Iraheta, E., Risselada, H. J., Milovanovic, D., Mueller, V., Müllar, S., Diederichsen, U., Fasshauer, D., Grubmüller, H., Hell, S. W., Eggeling, C., Kühnel, K., and Jahn, R. (2013) Phosphatidylinositol 4,5-bisphosphate clusters act as molecular beacons for vesicle recruitment. *Nat. Struct. Mol. Biol.* **20,** 679–686
15. Gowrishankar, K., Ghosh, S., Saha, S., C. R., Mayor, S., and Rao, M. (2012) Active remodeling of cortical actin regulates spatiotemporal organization of cell surface molecules. *Cell* **149,** 1353–1367
16. Veatch, S. L., and Keller, S. L. (2003) Separation of liquid phases in giant vesicles of ternary mixtures of phospholipids and cholesterol. *Biophys. J.* **85,** 3074–3083
17. Veatch, S. L., and Keller, S. L. (2003) A closer look at the canonical "raft mixture" in model membrane studies. *Biophys. J.* **84,** 725–726
18. Baumgart, T., Hess, S. T., and Webb, W. W. (2003) Imaging coexisting fluid domains in biomembrane models coupling curvature and line tension. *Nature* **425,** 821–824
19. Sengupta, P., Baird, B., and Holowka, D. (2007) Lipid rafts, fluid/fluid phase separation, and their relevance to plasma membrane structure and function. *Semin. Cell Dev. Biol.* **18,** 583–590
20. Levental, I., Byfield, F. J., Chowdhury, P., Gai, F., Baumgart, T., and Janmey, P. A. (2009) Cholesterol-dependent phase separation in cell-derived giant plasma-membrane vesicles. *Biochem. J.* **424,** 163–167
21. Esposito, C., Tian, A., Melamed, S., Johnson, C., Tee, S. Y., and Baumgart, T. (2007) Flicker spectroscopy of thermal lipid bilayer domain boundary fluctuations. *Biophys. J.* **93,** 3169–3181
22. London, E. (2005) How principles of domain formation in model membranes may explain ambiguities concerning lipid raft formation in cells. *Biochim. Biophys. Acta* **1746,** 203–220
23. London, E. (2002) Insights into lipid raft structure and formation from experiments in model membranes. *Curr. Opin. Struct. Biol.* **12,** 480–486
24. LaRocca, T. J., Pathak, P., Chiantia, S., Toledo, A., Silvius, J. R., Benach, J. L., and London, E. (2013) Proving lipid rafts exist: membrane domains in the prokaryote *Borrelia burgdorferi* have the same properties as eukaryotic lipid rafts. *PLoS Pathog.* **9,** e1003353
25. Simons, K., and Sampaio, J. L. (2011) Membrane organization and lipid rafts. *Cold Spring Harb. Perspect. Biol.* **3,** a004697
26. Simons, K., and Ehehalt, R. (2002) Cholesterol, lipid rafts, and disease. *J. Clin. Invest.* **110,** 597–603
27. Levental, I., Grzybek, M., and Simons, K. (2011) Raft domains of variable properties and compositions in plasma membrane vesicles. *Proc. Natl. Acad. Sci. U.S.A.* **108,** 11411–11416
28. Levental, I., Lingwood, D., Grzybek, M., Coskun, U., and Simons, K. (2010) Palmitoylation regulates raft affinity for the majority of integral raft proteins. *Proc. Natl. Acad. Sci. U.S.A.* **107,** 22050–22054
29. Sengupta, P., Hammond, A., Holowka, D., and Baird, B. (2008) Structural determinants for partitioning of lipids and proteins between coexisting fluid phases in giant plasma membrane vesicles. *Biochim. Biophys. Acta* **1778,** 20–32
30. Johnson, S. A., Stinson, B. M., Go, M. S., Carmona, L. M., Reminick, J. I., Fang, X., and Baumgart, T. (2010) Temperature-dependent phase behavior and protein partitioning in giant plasma membrane vesicles. *Biochim. Biophys. Acta* **1798,** 1427–1435
31. Zhao, J., Wu, J., and Veatch, S. L. (2013) Adhesion stabilizes robust lipid heterogeneity in supercritical membranes at physiological temperature. *Biophys. J.* **104,** 825–834
32. Veatch, S. L., Cicuta, P., Sengupta, P., Honerkamp-Smith, A., Holowka, D., and Baird, B. (2008) Critical fluctuations in plasma membrane vesicles. *ACS Chem. Biol.* **3,** 287–293
33. Zhou, Y., Cho, K. J., Plowman, S. J., and Hancock, J. F. (2012) Nonsteroidal anti-inflammatory drugs alter the spatiotemporal organization of Ras proteins on the plasma membrane. *J. Biol. Chem.* **287,** 16586–16595
34. Pralle, A., Keller, P., Florin, E. L., Simons, K., and Hörber, J. K. (2000) Sphingolipid-cholesterol rafts diffuse as small entities in the plasma membrane of mammalian cells. *J. Cell Biol.* **148,** 997–1008
35. Eggeling, C., Ringemann, C., Medda, R., Schwarzmann, G., Sandhoff, K., Polyakova, S., Belov, V. N., Hein, B., von Middendorff, C., Schönle, A., and Hell, S. W. (2009) Direct observation of the nanoscale dynamics of membrane lipids in a living cell. *Nature* **457,** 1159–1162
36. Prior, I. A., Harding, A., Yan, J., Sluimer, J., Parton, R. G., and Hancock, J. F. (2001) GTP-dependent segregation of H-Ras from lipid rafts is required for biological activity. *Nat. Cell Biol.* **3,** 368–375
37. Prior, I. A., Muncke, C., Parton, R. G., and Hancock, J. F. (2003) Direct visualization of Ras proteins in spatially distinct cell surface microdomains. *J. Cell Biol.* **160,** 165–170
38. Hancock, J. F. (2003) Ras proteins: different signals from different locations. *Nat. Rev. Mol. Cell Biol.* **4,** 373–384
39. Abankwa, D., Gorfe, A. A., Inder, K., and Hancock, J. F. (2010) Ras membrane orientation and nanodomain localization generate isoform diversity. *Proc. Natl. Acad. Sci. U.S.A.* **107,** 1130–1135
40. Inder, K., and Hancock, J. F. (2008) System output of the MAPK module is spatially regulated. *Commun. Integr. Biol.* **1,** 178–179
41. Inder, K., Harding, A., Plowman, S. J., Philips, M. R., Parton, R. G., and Hancock, J. F. (2008) Activation of the MAPK module from different spatial locations generates distinct system outputs. *Mol. Biol. Cell* **19,** 4776–4784
42. Zhou, Y., Hancock, J. F., and Lichtenberger, L. M. (2010) The nonsteroidal anti-inflammatory drug indomethacin induces heterogeneity in lipid membranes: potential implication for its diverse biological action. *PLoS One* **5,** e8811
43. Zhou, Y., Plowman, S. J., Lichtenberger, L. M., and Hancock, J. F. (2010) The anti-inflammatory drug indomethacin alters nanoclustering in synthetic and cell plasma membranes. *J. Biol. Chem.* **285,** 35188–35195
44. Akare, S., and Martinez, J. D. (2005) Bile acid induces hydrophobicity-dependent membrane alterations. *Biochim. Biophys. Acta* **1735,** 59–67
45. Jean-Louis, S., Akare, S., Ali, M. A., Mash, E. A., Jr., Meuillet, E., and Martinez, J. D. (2006) Deoxycholic acid induces intracellular signaling through membrane perturbations. *J. Biol. Chem.* **281,** 14948–14960
46. Powell, A. A., LaRue, J. M., Batta, A. K., and Martinez, J. D. (2001) Bile acid hydrophobicity is correlated with induction of apoptosis and/or growth arrest in HCT116 cells. *Biochem. J.* **356,** 481–486
47. Kim, H. M., Choo, H. J., Jung, S. Y., Ko, Y. G., Park, W. H., Jeon, S. J., Kim, C. H., Joo, T., and Cho, B. R. (2007) A two-photon fluorescent probe for lipid raft imaging: C-Laurdan. *Chembiochem* **8,** 553–559
48. Zhou, Y., Doyen, R., and Lichtenberger, L. M. (2009) The role of membrane cholesterol in determining bile acid cytotoxicity and cytoprotection of ursodeoxycholic acid. *Biochim. Biophys. Acta* **1788,** 507–513
49. Zhou, Y., Dial, E. J., Doyen, R., and Lichtenberger, L. M. (2010) Effect of indomethacin on bile acid-phospholipid interactions: implication for small intestinal injury induced by nonsteroidal anti-inflammatory drugs. *Am. J. Physiol. Gastrointest. Liver Physiol.* **298,** G722–731
50. Sezgin, E., Kaiser, H. J., Baumgart, T., Schwille, P., Simons, K., and Levental, I. (2012) Elucidating membrane structure and protein behavior using giant plasma membrane vesicles. *Nat. Protoc.* **7,** 1042–1051
51. Kaiser, H. J., Lingwood, D., Levental, I., Sampaio, J. L., Kalvodova, L., Rajendran, L., and Simons, K. (2009) Order of lipid phases in model and plasma membranes. *Proc. Natl. Acad. Sci. U.S.A.* **106,** 16645–16650
52. Roda, A., Hofmann, A. F., and Mysels, K. J. (1983) The influence of bile salt structure on self-association in aqueous solutions. *J. Biol. Chem.* **258,** 6362–6370
53. Levental, I., Grzybek, M., and Simons, K. (2010) Greasing their way: lipid modifications determine protein association with membrane rafts. *Biochemistry* **49,** 6305–6316
54. Carón, R. W., Yacoub, A., Li, M., Zhu, X., Mitchell, C., Hong, Y., Hawkins, W., Sasazuki, T., Shirasawa, S., Kozikowski, A. P., Dennis, P. A., Hagan, M. P., Grant, S., and Dent, P. (2005) Activated forms of H-Ras and K-Ras differentially regulate membrane association of PI3K, PDK-1, and AKT and the effect of therapeutic kinase inhibitors on cell survival. *Mol. Cancer Ther.* **4,** 257–270
55. Choi, J. A., Park, M. T., Kang, C. M., Um, H. D., Bae, S., Lee, K. H., Kim,

T. H., Kim, J. H., Cho, C. K., Lee, Y. S., Chung, H. Y., and Lee, S. J. (2004) Opposite effects of Ha-Ras and Ki-Ras on radiation-induced apoptosis via differential activation of PI3K/Akt and Rac/p38 mitogen-activated protein kinase signaling pathways. *Oncogene* **23,** 9–20

56. Kaiser, H. J., Surma, M. A., Mayer, F., Levental, I., Grzybek, M., Klemm, R. W., Da Cruz, S., Meisinger, C., Müller, V., Simons, K., and Lingwood, D. (2011) Molecular convergence of bacterial and eukaryotic surface order. *J. Biol. Chem.* **286,** 40631–40637
57. Simons, K., and Ikonen, E. (1997) Functional rafts in cell membranes. *Nature* **387,** 569–572
58. Simons, K., and Vaz, W. L. (2004) Model systems, lipid rafts, and cell membranes. *Annu. Rev. Biophys. Biomol. Struct.* **33,** 269–295
59. Mello-Vieira, J., Sousa, T., Coutinho, A., Fedorov, A., Lucas, S. D., Moreira, R., Castro, R. E., Rodrigues, C. M., Prieto, M., and Fernandes, F. (2013) Cytotoxic bile acids, but not cytoprotective species, inhibit the ordering effect of cholesterol in model membranes at physiologically active concentrations. *Biochim. Biophys. Acta* **1828,** 2152–2163
60. Nichols, J. W. (1986) Low concentrations of bile salts increase the rate of spontaneous phospholipid transfer between vesicles. *Biochemistry* **25,** 4596–4601
61. Plowman, S. J., Muncke, C., Parton, R. G., and Hancock, J. F. (2005) H-ras, K-ras, and inner plasma membrane raft proteins operate in nanoclusters with differential dependence on the actin cytoskeleton. *Proc. Natl. Acad. Sci. U.S.A.* **102,** 15500–15505
62. Scotti, E., Gilardi, F., Godio, C., Gers, E., Krneta, J., Mitro, N., De Fabiani, E., Caruso, D., and Crestani, M. (2007) Bile acids and their signaling pathways: eclectic regulators of diverse cellular functions. *Cell Mol. Life Sci.* **64,** 2477–2491